International Journal of Solids and Structures 48 (2011) 2668–2680

Contents lists available at ScienceDirect

International Journal of Solids and Structures

journal homepage: www.elsevier.com/locate/ijsolstr

# Homogenization of aligned "fuzzy fiber" composites

George Chatzigeorgiou [a], Yalchin Efendiev [b], Dimitris C. Lagoudas [a,*]

[a] Dept. of Aerospace Engineering, Texas A&M University, College Station, TX 77843, USA
[b] Dept. of Mathematics, Texas A&M University, College Station, TX 77843, USA

ARTICLE INFO

*Article history:*
Received 2 February 2011
Received in revised form 13 May 2011
Available online 26 May 2011

*Keywords:*
Carbon fibers
Carbon nanotubes
Asymptotic expansion homogenization method

ABSTRACT

The aim of this work is to study composites in which carbon fibers coated with radially aligned carbon nanotubes are embedded in a matrix. The effective properties of these composites are identified using the asymptotic expansion homogenization method in two steps. Homogenization is performed in different coordinate systems, the cylindrical and the Cartesian, and a numerical example are presented.



## 1. Introduction

Despite their recent discovery by Iijima (1991), the carbon nanotubes (CNTs) have attracted considerable research attention. Nowadays a large variety of composites containing CNTs have been manufactured (Milo et al., 1999; Peigney et al., 2000; Potschke et al., 2004; Wagner et al., 1998; Lourie and Wagner, 1998; Star et al., 2001; McCarthy et al., 2002; Zhu et al., 2003). This scientific interest is derived from the CNTs exceptional properties. Carbon nanotubes are reported to have an axial Young's modulus in the range of 300–1000 GPa, up to five times the stiffness and with half the density of SiC fibers, while their theoretical elongation to break reaches 30–40% (Yakobson and Smalley, 1997; Yakobson et al., 1997; Yu et al., 2000; Wang et al., 2001; Salvetat-Delmotte and Rubio, 2002; Fisher et al., 2002; Popov, 2004).

Modeling of composites containing CNTs has also grown significantly in recent years. The mechanical response in tension of a single CNT embedded in polymer via finite element analysis was studied by Liu and Chen (2003a), while (Odegard et al., 2003) modeled aligned and misaligned CNT composites using the equivalent continuum method in conjunction with the Mori–Tanaka micromechanics method. Fisher et al. (2002, 2003) studied the effects of nanotube waviness on the effective composite properties using finite element analysis and the micromechanics Mori–Tanaka method. Hadjiev et al. (2006) considered buckling of CNTs within an epoxy matrix. Several efforts in CNT composite modeling have focused on the inclusion of less than ideal CNT adhesion to the matrix (Wagner, 2002; Frankland et al., 2003; Griebel and Hamaekers, 2004). The clustering of CNTs in the polymer matrix was studied in Seidel and Lagoudas (2006). In Spanos and Kontsos (2008) nanocomposite properties were computed using Monte Carlo finite element method. Molecular dynamics (MD) simulations have been used to obtain the stress–strain behavior of CNTs embedded in a polymer matrix (Frankland et al., 2002), or the properties of the interphase between CNTs and polymer (Awasthi et al., 2009). In all these modeling efforts, the carbon nanotubes are embedded directly in a polymer matrix.

In this work we focus on composites containing carbon fibers, which are coated with carbon nanotubes ("fuzzy fibers"). In order to achieve significant enhancement of the mechanical behavior of the interface between the carbon fiber and the matrix, we choose to work with "fuzzy fibers" where the CNTs are radially aligned on the surface of the carbon fibers. In these composites, the interphase layer between the fiber and the matrix can be seen as a separate composite material consisting of CNTs in radial arrangement inside a matrix. In this perspective, the "fuzzy fiber" can be studied as a two concentric cylinders material, the fiber and the interphase layer. The elastic response of homogeneous and non-homogeneous cylinders under different boundary conditions was studied by Chatterjee (1970, 1999a,b), Chen et al. (2000), Tarn and Wang (2001), Tarn (2002), Ruhi et al. (2005), Hosseini Kordkheili and Naghdabadi (2007), Chatzigeorgiou et al. (2008), Tsukrov and Drach (2010), Nie and Batra (2010a,b,c).

Our goal is to obtain the effective mechanical properties of unidirectional "fuzzy fiber" composites. In order to achieve it we use a multiscale approach based on the asymptotic expansion homogenization method (AEH). The AEH method is well documented in the literature for periodic composites (Sanchez-Palencia, 1978; Bensoussan et al., 1978; Kalamkarov and Kolpakov, 1997;

* Corresponding author.
*E-mail address:* lagoudas@tamu.edu (D.C. Lagoudas).

0020-7683/$ - see front matter © 2011 Elsevier Ltd. All rights reserved.
doi:10.1016/j.ijsolstr.2011.05.011

Chung et al., 2001), whose periodicity can be represented in the Cartesian coordinate system. In this paper, due to the structure of the interphase layer (angular periodicity), we present a modified version of the AEH method, in which the homogenized properties of the composite are obtained in two steps. Initially, the properties of the interphase layer are computed through homogenization with respect to a cylindrical coordinate system. Then, the homogenized layer is introduced in the actual "fuzzy fiber" composite, which is homogenized with respect to a Cartesian coordinate system.

The structure of this paper is the following: in Section 2 we describe the characteristics of the "fuzzy fiber" composites and the mathematical assumptions. The first step of homogenization, which refers to the nanocomposite layer of a "fuzzy fiber" is presented in Section 3. Section 4 discusses the second step of homogenization in the mesoscale. A numerical example is presented in Section 5, in which the effective properties of a "fuzzy fiber" are obtained and local stresses at the microscale level are computed. The final section includes the major conclusions.

## 2. "Fuzzy fiber" composites

The "fuzzy fiber" composite we want to study is a fiber composite material system, in which a carbon fiber (CF) is coated with radially aligned carbon nanotubes (CNTs) (Fig. 1). The "fuzzy fiber" is embedded in a matrix, which can be an epoxy. The intermediate layer between the CF and the matrix, consisting of CNTs and matrix, will be denoted in the sequel as nanocomposite (NCP). The CF is represented here as a long cylinder, while the CNTs are represented as hollow tubes of very large length, compared to their diameter.

The composite we investigate consists of unidirectional "fuzzy fibers", distributed in a hexagonal form inside the matrix (Fig. 2). The hexagonal distribution efficiently represents a random distribution of the fibers in the matrix (Hashin and Rosen, 1964).

In order to obtain the effective properties of the composite, we are using the asymptotic expansion homogenization (AEH) method, which is a two scale homogenization method. The AEH is a well established method (Sanchez-Palencia, 1978; Bensoussan et al., 1978; Kalamkarov and Kolpakov, 1997), in which 2 scales are taken into account, the macroscale and the microscale. In a Cartesian coordinate system framework, the macroscale is described by the coordinates $(x_1,x_2,x_3)$, while the microscale by the coordinates $\left(\frac{x_1}{\epsilon},\frac{x_2}{\epsilon},\frac{x_3}{\epsilon}\right)$, where $\epsilon$ is the characteristic length of the periodic cell. The idea of the method is that the displacements are written in an asymptotic series form with respect to $\epsilon$ and the expanded forms of the equilibrium equations lead to $\epsilon^{-1}$ terms (microequations) and $\epsilon^0$ terms (macroequations). From the microequations we obtain the necessary quantities, whose averages give us the homogenized properties used in the macroequations.

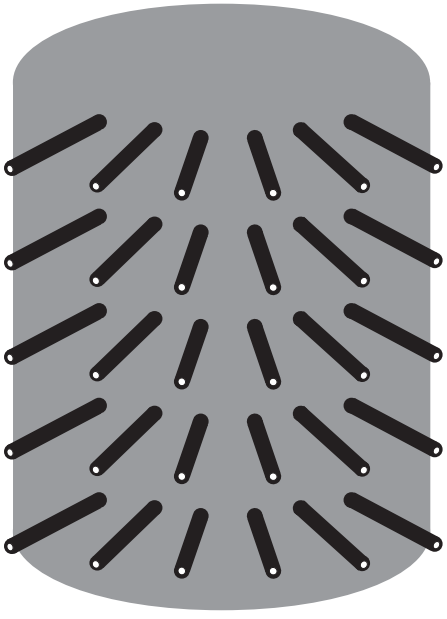

**Fig. 1.** "Fuzzy fiber": Carbon fiber coated with radially aligned carbon nanotubes.

In our composite system, the unit cell of Fig. 2b consists of 3 different material systems, the carbon fiber, the nanocomposite and the matrix. The nanocomposite though by itself is a composite (Fig. 3a), whose periodic cell is represented in a cylindrical coordinate system. Its structure can include CNTs in tetragonal (Fig. 3b) or hexagonal (Fig. 3c) array. In this case, in addition to the characteristic length $\epsilon$, we need to introduce the characteristic length of the nanocomposite $\delta$. This leads to three series of coordinates, the macroscale $(x_1,x_2,x_3)$, the mesoscale $\left(\frac{x_1}{\epsilon},\frac{x_2}{\epsilon},\frac{x_3}{\epsilon}\right)$ and the microscale $\left(\frac{x_1}{\delta},\frac{x_2}{\delta},\frac{x_3}{\delta}\right)$. The characteristic lengths $\delta$ and $\epsilon$ can be related with one as the square power of the other. In this work though we prefer to use two independent characteristic lengths, in order to allow the independency of the two scales. Since the AEH method is based on the idea of $\epsilon$ or $\delta$ tending to zero, the microscale characteristic length $\delta$ and the mesoscale characteristic length $\epsilon$ can be seen as independently tending to zero. If one of the two characteristic lengths is not close to zero (for instance, if we have very few CNTs in the nanocomposite, $\delta$ is not close to zero) then the homogenization in this scale is not necessarily accurate.

In order to solve efficiently this 3 scale problem, we split it into two 2 scale problems. The first problem is describing the relation between the microscale and the mesoscale, and focuses in the computation of the effective properties of the NCP. The NCP effective properties are used in the second problem which deals with the connection between the mesoscale and the macroscale.

The homogenization of a "fuzzy fiber" composite can be put into a general framework of homogenization with multiple metrics. As in homogenization of a "fuzzy fiber" composite, there are many applications where small-scale features can have periodic or regular forms that can be handled with existing homogenization techniques. For example, one may need to select a certain coordinate system at a given scale to have periodicity or sufficient regularity. We will discuss some examples after presenting the homogenization. Consider a material whose properties are defined on $N$ different scales

$$C\left(\frac{x}{\epsilon_1},\frac{x}{\epsilon_2},\ldots,\frac{x}{\epsilon_N}\right),$$

where we do not assume a periodicity at any scales. Assume that the periodicity can be achieved at any of the scales if one can consider an appropriate coordinate system. For example, the cylindrical coordinate system provides periodic microstructure at the scale $N$, while for the scale $N-1$, we may need to choose the spherical coordinate system to achieve periodicity at that scale. Any coordinate system is defined via a metric tensor $G=(g_{ij})$. We denote the metric that gives homogenization-amenable coordinate system for $i$th scale by $G_i$. Then, we re-write our material properties as

$$C\left(\frac{x^{G_1}}{\epsilon_1},\frac{x^{G_2}}{\epsilon_2},\ldots,\frac{x^{G_N}}{\epsilon_N}\right), \tag{1}$$

where $\epsilon_N \ll \cdots \ll \epsilon_1$ and $G_i$'s are the metrics for $i$th coordinate system where homogenization is performed.

As we mentioned above that the metric elements $G=(g_{ij})$ can correspond to some well-known coordinate transformations (e.g., spherical or cylindrical) or can be non-trivial transformations as

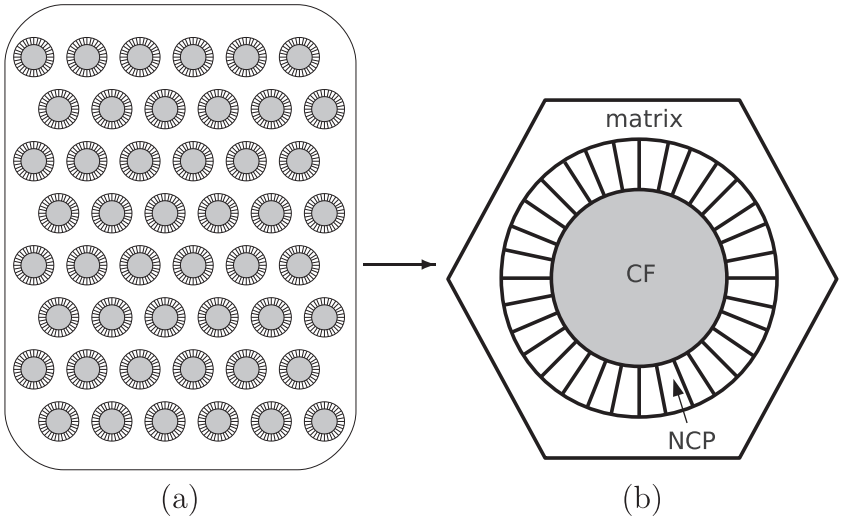


**Fig. 2.** (a) "Fuzzy fiber" composite and (b) unit cell of the composite.

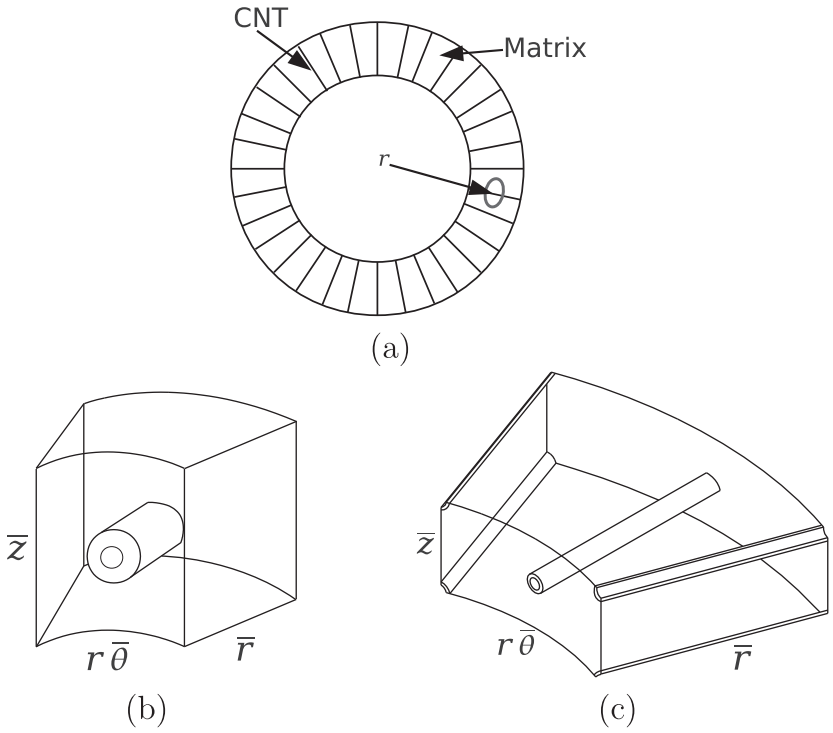


**Fig. 3.** (a) Cross section of the nanocomposite, (b) tetragonal unit cell of the nanocomposite and (c) hexagonal unit cell of the nanocomposite.

in the case of problems without scale separation (Owhadi and Zhang, 2007; Efendiev and Hou, 2009). In Owhadi and Zhang (2007) it was shown that in the case of no-scale separation, by choosing the metric correctly, one can smooth the solution and thus, the solution can be approximated by piecewise linear functions on new coordinate system. The metric here is defined via a solution of cell problems in a large domain. Consequently, in general, one needs to consider appropriate metrics at different scales to take advantage of the regularity of the solution or special features.

To carry out the homogenization in a media where different coordinate metrics are used at different scales, we start the homogenization from the smallest scale by freezing coordinates in all larger scales. Once the homogenization is performed at the corresponding metric, the material properties are transformed to the metric of the next scale. One requirement is that the metric needs not to vary rapidly at the scale of the homogenized variable so that when transforming to the next coordinate system, the smallest scales are removed. More precisely, assume that the scale $\epsilon_N$ is being homogenized in the metric $G_N$. Then,

$$C^*\left(\frac{x^{G_1}}{\epsilon_1},\frac{x^{G_2}}{\epsilon_2},\ldots,\frac{x^{G_{N-1}}}{\epsilon_N}\right)=H_{G_N}\left(C\left(\frac{x^{G_1}}{\epsilon_1},\frac{x^{G_2}}{\epsilon_2},\ldots,\frac{x^{G_N}}{\epsilon_N}\right)\right),$$

where $H_{G_N}$ is the homogenization operator (generally, nonlinear operator) in coordinate system with metric $G_N$. To do this homogenization, coefficients are frozen at the scales $\epsilon_1,\ldots,\epsilon_{N-1}$, and then transformed to the coordinate system with the metric $G_N$. At this

scale, the coefficients are homogenized and then transformed to $G_{N-1}$. One needs to ensure that this transformation does not bring back $\epsilon_N$ scale. For this reason we need to assume that $G_N$ does not depend on $\epsilon_N$, i.e., the transformation metric does not vary rapidly at the scale $\epsilon_N$. The mathematical error analysis will require some additional conditions on metrics such as boundedness of the transformation tensor. In this paper, our new framework is applied to an example problem.

## 3. Nanocomposite layer of a "fuzzy fiber" composite

In this section we are going to investigate the effective properties of the NCP. This intermediate layer of the "fuzzy fibers" composites consists of radially aligned CNTs and matrix (Fig. 3a). The unit cell of the NCP is shown in Fig. 3b. The effective mechanical properties of the nanocomposite will be obtained using the asymptotic expansion homogenization method. In this approach two scales are considered, the mesoscale and the microscale with characteristic length $\delta$. In cylindrical coordinates we have the meso coordinates $(r,\theta,z)$[1] and the micro coordinates $\left(\frac{r}{\delta},\frac{\theta}{\delta},\frac{z}{\delta}\right)\to(\bar{r},\bar{\theta},\bar{z})$. The choice of the cylindrical coordinate system has two main advantages: (a) due to the NCP structure, there is no fast variation in the radial direction, reducing the microscale equations to 2-D, (b) allows us to represent in a rigorous way the homogenization procedure and (c) the periodicity of the microstructure is represented easier with respect to $\bar{\theta}$ and $\bar{z}$. For clarity and simplification, we denote the axes $(r,\theta,z)$ as $(1,2,3)$ and we use the Einstein summation rule for double indices. Additionally, we introduce the operators $\mathcal{L}_i$ for the mesoscale and $\overline{\mathcal{L}}_i$ for the microscale, where

$$\mathcal{L}_1=\frac{\partial}{\partial r},\quad \mathcal{L}_2=\frac{1}{r}\frac{\partial}{\partial\theta},\quad \mathcal{L}_3=\frac{\partial}{\partial z}, \tag{2}$$

$$\overline{\mathcal{L}}_1=\frac{\partial}{\partial\bar{r}},\quad \bar{\mathcal{L}}_2=\frac{1}{r}\frac{\partial}{\partial\bar{\theta}},\quad \bar{\mathcal{L}}_3=\frac{\partial}{\partial\bar{z}}. \tag{3}$$

The aim of the asymptotic expansion homogenization (AEH) method is to identify the behavior of the composite material, when the size of the microstructure becomes infinitesimally small, i.e., $\delta\to 0$. In all the quantities (displacements, strains, stresses, stiffness components) we will use the superscript $\delta$, denoting that we refer to a material point, which can be in the matrix, in the CNT or in the void. The strain-displacement relation of the material system in cylindrical coordinates read[2]

$$\begin{aligned}
&\hat{\varepsilon}^\delta_{11}=\mathcal{L}_1\hat{u}^\delta_1,\quad \hat{\varepsilon}^\delta_{22}=\mathcal{L}_2\hat{u}^\delta_2+\frac{\hat{u}^\delta_1}{r},\quad \hat{\varepsilon}^\delta_{33}=\mathcal{L}_3\hat{u}^\delta_3,\\
&\hat{\varepsilon}^\delta_{23}=\frac{1}{2}\left(\mathcal{L}_2\hat{u}^\delta_3+\mathcal{L}_3\hat{u}^\delta_2\right),\quad \hat{\varepsilon}^\delta_{13}=\frac{1}{2}\left(\mathcal{L}_1\hat{u}^\delta_3+\mathcal{L}_3\hat{u}^\delta_1\right),\\
&\hat{\varepsilon}^\delta_{12}=\frac{1}{2}\left(\mathcal{L}_1\hat{u}^\delta_2+\mathcal{L}_2\hat{u}^\delta_1-\frac{\hat{u}^\delta_2}{r}\right).
\end{aligned} \tag{4}$$

Ignoring inertia and body forces, the equilibrium equations are written as

$$\mathcal{L}_j\hat{\sigma}^\delta_{1j}+\frac{\hat{\sigma}^\delta_{11}-\hat{\sigma}^\delta_{22}}{r}=0,\quad \mathcal{L}_j\hat{\sigma}^\delta_{2j}+2\frac{\hat{\sigma}^\delta_{12}}{r}=0,\quad \mathcal{L}_j\hat{\sigma}^\delta_{3j}+\frac{\hat{\sigma}^\delta_{13}}{r}=0. \tag{5}$$

Finally, the Hooke's law is written

$$\hat{\sigma}^\delta_{ij}=\widehat{C}^\delta_{ijkl}\hat{\varepsilon}^\delta_{kl}. \tag{6}$$

The stiffness components $\widehat{C}^\delta_{ijkl}$ are generally spatially dependent. At the microscale level it depends on the microcoordinates $\bar{\theta}$ and $\bar{z}$. The material parameters vary very slowly in the radial direction and depend on the mesocoordinate $r$. Due to the geometry of the CNT (only its center is independent on $r$), the stiffness components present local discontinuity with respect to $r$. The discontinuity appears only when we move from the void to the CNT and from the CNT to the matrix. So we can write

$$\widehat{C}^\delta_{ijkl}=\widehat{C}^\delta_{ijkl}(r,\bar{\theta},\bar{z}),\quad \text{slow variation with respect to } r. \tag{7}$$

In the AEH method, the displacements are represented in a series expansion form

$$\hat{u}^\delta_i=\hat{u}^{(0)}_i(r,\theta,z)+\delta\hat{u}^{(1)}_i(r,\theta,z,\bar{\theta},\bar{z})+\delta^2\hat{u}^{(2)}_i(r,\theta,z,\bar{\theta},\bar{z})+\cdots, \tag{8}$$

where $\hat{u}^{(0)}_i$ denotes the mesodisplacement and $\hat{u}^{(1)}_i$, $\hat{u}^{(2)}_i$ e.t.c. are periodic functions and represent the oscillating terms. The derivatives can be written in the form

$$\mathcal{L}_i=\mathcal{L}_i+\frac{1}{\delta}\overline{\mathcal{L}}_i. \tag{9}$$

Using (8) and (9), the strains in (4) can be written in the form

$$\hat{\varepsilon}^\delta_{ij}=\hat{\varepsilon}^{(0)}_{ij}+\delta\hat{\varepsilon}^{(1)}_{ij}+\cdots, \tag{10}$$

where

$$\hat{\varepsilon}^{(m)}_{ij}=\hat{\varepsilon}^{(m*)}_{ij}+\frac{1}{2}\left(\overline{\mathcal{L}}_i\hat{u}^{(m+1)}_j+\overline{\mathcal{L}}_j\hat{u}^{(m+1)}_i\right),\quad m=0,1,2,\ldots \tag{11}$$

and

$$\begin{aligned}
&\hat{\varepsilon}^{(m*)}_{11}=\mathcal{L}_1\hat{u}^{(m)}_1,\quad \hat{\varepsilon}^{(m*)}_{22}=\mathcal{L}_2\hat{u}^{(m)}_2+\frac{\hat{u}^{(m)}_1}{r},\quad \hat{\varepsilon}^{(m*)}_{33}=\mathcal{L}_3\hat{u}^{(m)}_3,\\
&\hat{\varepsilon}^{(m*)}_{23}=\frac{1}{2}\left(\mathcal{L}_3\hat{u}^{(m)}_2+\mathcal{L}_2\hat{u}^{(m)}_3\right),\quad \hat{\varepsilon}^{(m*)}_{13}=\frac{1}{2}\left(\mathcal{L}_1\hat{u}^{(m)}_3+\mathcal{L}_3\hat{u}^{(m)}_1\right),\\
&\hat{\varepsilon}^{(m*)}_{12}=\frac{1}{2}\left(\mathcal{L}_2\hat{u}^{(m)}_1+\mathcal{L}_1\hat{u}^{(m)}_2-\frac{\hat{u}^{(m)}_2}{r}\right).
\end{aligned} \tag{12}$$

From the Hooke's law (6) and (10) we can write the expanded form of the stresses

$$\hat{\sigma}^\delta_{ij}=\hat{\sigma}^{(0)}_{ij}+\delta\hat{\sigma}^{(1)}_{ij}+\cdots, \tag{13}$$

where

$$\hat{\sigma}^{(m)}_{ij}=\widehat{C}_{ijkl}\hat{\varepsilon}^{(m*)}_{kl}+\widehat{C}_{ijkl}\overline{\mathcal{L}}_k\hat{u}^{(m+1)}_l. \tag{14}$$

Using the expanded form of the stresses (13) and the Eq. (9) the equilibrium equations take the form

$$\frac{1}{\delta}\left(\overline{\mathcal{L}}_j\hat{\sigma}^{(0)}_{1j}\right)+\mathcal{L}_j\hat{\sigma}^{(0)}_{1j}+\frac{\hat{\sigma}^{(0)}_{11}-\hat{\sigma}^{(0)}_{22}}{r}+\bar{\mathcal{L}}_j\hat{\sigma}^{(1)}_{1j}+\delta\cdots=0, \tag{15}$$

$$\frac{1}{\delta}\left(\overline{\mathcal{L}}_j\hat{\sigma}^{(0)}_{2j}\right)+\mathcal{L}_j\hat{\sigma}^{(0)}_{2j}+2\frac{\hat{\sigma}^{(0)}_{12}}{r}+\bar{\mathcal{L}}_j\hat{\sigma}^{(1)}_{2j}+\delta\cdots=0, \tag{16}$$

$$\frac{1}{\delta}\left(\overline{\mathcal{L}}_j\hat{\sigma}^{(0)}_{3j}\right)+\mathcal{L}_j\hat{\sigma}^{(0)}_{3j}+\frac{\hat{\sigma}^{(0)}_{13}}{r}+\bar{\mathcal{L}}_j\hat{\sigma}^{(1)}_{3j}+\delta\cdots=0. \tag{17}$$

According to the classical procedure of the AEH method, the micro-equations are defined from the $\delta^{-1}$ terms

$$\overline{\mathcal{L}}_j\hat{\sigma}^{(0)}_{ij}=0,\quad i=1,2,3, \tag{18}$$

which, using Eq. (14) for $m=0$, can be written as

$$\overline{\mathcal{L}}_j\left(\widehat{C}_{ijkl}\right)\hat{\varepsilon}^{(0*)}_{kl}+\overline{\mathcal{L}}_j\left(\widehat{C}_{ijkl}\overline{\mathcal{L}}_k\hat{u}^{(1)}_l\right)=0. \tag{19}$$

In Eq. (19) $\hat{\varepsilon}^{(0*)}_{ij}$ depends only on the meso-displacements $\hat{u}^{(0)}_i$. By assuming that

$$\hat{u}^{(1)}_i=\widehat{N}^{mn}_i\hat{\varepsilon}^{(0*)}_{mn}, \tag{20}$$

the micro-Eq. (19) are written

[1] For simplicity in the expressions, we omit the mesoscale characteristic length $\epsilon$.

[2] In the sequel, we will use $\hat{}$ to denote that the specific quantity refers to cylindrical coordinate system.

$$\overline{\mathcal{L}}_j\left(\widehat{C}_{ijmn}+\widehat{C}_{ijkl}\overline{\mathcal{L}}_k\widehat{N}_l^{mn}\right)=0. \tag{21}$$

The final form of the micro-equations are solved for the unknown functions $\widehat{N}_i^{mn}$, which are periodic in the $(\bar{\theta},\bar{z})$ space. Also, we need to impose the necessary continuity conditions

$$[\![\widehat{N}_i^{mn}]\!]=0,[\![\left(\widehat{C}_{ijmn}+\widehat{C}_{ijkl}\overline{\mathcal{L}}_k\widehat{N}_l^{mn}\right)n_j]\!]=0, \tag{22}$$

where $n_i$ is the unit normal vector to the surface of discontinuity.

The meso-equations can be obtained from the $\delta^0$ terms of the equilibrium equations. When $\delta$ approaches zero, periodic functions attain their weak limit, which is equal to the area integral of the functions in the periodic unit cell. We introduce the area integral symbol on the area $A$ of the 2-D unit cell in $(\bar{\theta},\bar{z})$,

$$\langle\phi\rangle=\frac{1}{A}\int_{-\bar{z}'/2}^{\bar{z}'/2}\int_{-\bar{\theta}'/2}^{\bar{\theta}'/2}r\phi(r,\bar{\theta},\bar{z})\mathrm{d}\bar{\theta}\,\mathrm{d}\bar{z}. \tag{23}$$

By setting $\omega_i$ as the outer unit normal vector to the boundary and $\partial A$ the boundary surface of the unit cell, we can use the Gauss theorem and the periodicity of $\hat{\sigma}_{ij}^{(1)}$ to show that

$$\left\langle\overline{\mathcal{L}}_j\hat{\sigma}_{ij}^{(1)}\right\rangle=\frac{r}{A}\int_{\partial A}\hat{\sigma}_{ij}^{(1)}\omega_j\,\mathrm{d}S=0. \tag{24}$$

The meso-equations then are obtained from the weak limit of the $\delta^0$ terms of the equilibrium equations

$$\begin{aligned}&\mathcal{L}_j\langle\hat{\sigma}_{1j}^{(0)}\rangle+\frac{\langle\hat{\sigma}_{11}^{(0)}\rangle-\langle\hat{\sigma}_{22}^{(0)}\rangle}{r}=0,\quad \mathcal{L}_j\langle\hat{\sigma}_{2j}^{(0)}\rangle+2\frac{\langle\hat{\sigma}_{12}^{(0)}\rangle}{r}=0,\\&\mathcal{L}_j\langle\hat{\sigma}_{3j}^{(0)}\rangle+\frac{\langle\hat{\sigma}_{13}^{(0)}\rangle}{r}=0,\end{aligned} \tag{25}$$

where

$$\left\langle\hat{\sigma}_{ij}^{(0)}\right\rangle=\left\langle\widehat{C}_{ijmn}+\widehat{C}_{ijkl}\overline{\mathcal{L}}_k\widehat{N}_l^{mn}\right\rangle\hat{\varepsilon}_{mn}^{(0*)}. \tag{26}$$

From the last equation it becomes obvious that the effective, or homogenized, properties $\widehat{C}_{ijkl}^{\mathrm{NCP}}$ are given by

$$\widehat{C}_{ijmn}^{\mathrm{NCP}}=\left\langle\widehat{C}_{ijmn}+\widehat{C}_{ijkl}\overline{\mathcal{L}}_k\widehat{N}_l^{mn}\right\rangle, \tag{27}$$

where the functions $\widehat{N}_i^{mn}$ are determined by solving the Eq. (21). It is important to note that one can possibly derive the homogenized equations using curvilinear periodicity cells. However, our approach provides a rigorous foundation of performing homogenization in curvilinear system.

In the microlevel and at a specific radius $r$, Eq. (21) represent 2 anti-plane strain problems and 4 plane strain problems. Due to the large difference in $\bar{\theta}$ and $\bar{z}$ scales, it is more preferable to solve the microequations in the $r\bar{\theta}-\bar{z}$. In the sequel, we will use $\hat{y}_2^*$ for the $r\bar{\theta}$ coordinate and $\hat{y}_3$ for the $\bar{z}$ coordinate and we will adopt the Voigt notation.[3] In the 2-D form, the anti-plane problems are given for $i=1$, $\alpha=5,6$

$$\begin{aligned}&-\frac{\partial}{\partial\hat{y}_2^*}\left(\widehat{C}_{66}\frac{\partial\widehat{N}_1^{\alpha}}{\partial\hat{y}_2^*}+\widehat{C}_{56}\frac{\partial\widehat{N}_1^{\alpha}}{\partial\hat{y}_3}\right)-\frac{\partial}{\partial\hat{y}_3}\left(\widehat{C}_{56}\frac{\partial\widehat{N}_1^{\alpha}}{\partial\hat{y}_2^*}+\widehat{C}_{55}\frac{\partial\widehat{N}_1^{\alpha}}{\partial\hat{y}_3}\right)\\&=\frac{\partial\widehat{C}_{6\alpha}}{\partial\hat{y}_2^*}+\frac{\partial\widehat{C}_{5\alpha}}{\partial\hat{y}_3},\end{aligned} \tag{28}$$

[3] We note that the Voigt notation is a way to rewrite a fourth order symmetric tensor $A_{ijkl}$ in a $6\times6$ matrix form $A_{\alpha\beta}$, by applying the substitutions: $11\to1$, $22\to2$, $33\to3$, $23\to4$, $13\to5$, $12\to6$.

The plane strain problems are given for $i=2$ and $i=3$, $\alpha=1,2,3,4$ from the system of equations

$$\begin{aligned}&-\frac{\partial}{\partial\hat{y}_2^*}\left(\widehat{C}_{22}\frac{\partial\widehat{N}_2^{\alpha}}{\partial\hat{y}_2^*}+\widehat{C}_{24}\frac{\partial\widehat{N}_2^{\alpha}}{\partial y_3}+\widehat{C}_{24}\frac{\partial\widehat{N}_3^{\alpha}}{\partial y_2^*}+\widehat{C}_{23}\frac{\partial\widehat{N}_3^{\alpha}}{\partial\hat{y}_3}\right)\\&-\frac{\partial}{\partial\hat{y}_3}\left(\widehat{C}_{24}\frac{\partial\widehat{N}_2^{\alpha}}{\partial\hat{y}_2^*}+C_{44}\frac{\partial\widehat{N}_2^{\alpha}}{\partial\hat{y}_3}+\widehat{C}_{44}\frac{\partial\widehat{N}_3^{\alpha}}{\partial\hat{y}_2^*}+\widehat{C}_{34}\frac{\partial\widehat{N}_3^{\alpha}}{\partial\hat{y}_3}\right)\\&=\frac{\partial\widehat{C}_{2\alpha}}{\partial\hat{y}_2^*}+\frac{\partial\widehat{C}_{4\alpha}}{\partial\hat{y}_3}.\end{aligned} \tag{29}$$

and

$$\begin{aligned}&-\frac{\partial}{\partial\hat{y}_2^*}\left(\widehat{C}_{24}\frac{\partial\widehat{N}_2^{\alpha}}{\partial\hat{y}_2^*}+\widehat{C}_{44}\frac{\partial\widehat{N}_2^{\alpha}}{\partial\hat{y}_3}+\widehat{C}_{44}\frac{\partial\widehat{N}_3^{\alpha}}{\partial\hat{y}_2^*}+\widehat{C}_{34}\frac{\partial\widehat{N}_3^{\alpha}}{\partial\hat{y}_3}\right)\\&-\frac{\partial}{\partial\hat{y}_3}\left(\widehat{C}_{23}\frac{\partial\widehat{N}_2^{\alpha}}{\partial\hat{y}_2^*}+\widehat{C}_{34}\frac{\partial\widehat{N}_2^{\alpha}}{\partial\hat{y}_3}+\widehat{C}_{34}\frac{\partial\widehat{N}_3^{\alpha}}{\partial\hat{y}_2^*}+\widehat{C}_{33}\frac{\partial\widehat{N}_3^{\alpha}}{\partial\hat{y}_3}\right)\\&=\frac{\partial\widehat{C}_{4\alpha}}{\partial\hat{y}_2^*}+\frac{\partial\widehat{C}_{3\alpha}}{\partial\hat{y}_3}.\end{aligned} \tag{30}$$

The effective properties of the nanocomposite are obtained by the relations

$$\begin{aligned}\widehat{C}_{1\alpha}^{\mathrm{NCP}}&=\left\langle\widehat{C}_{1\alpha}+\widehat{C}_{12}\frac{\partial\widehat{N}_2^{\alpha}}{\partial\hat{y}_2^*}+\widehat{C}_{14}\frac{\partial\widehat{N}_2^{\alpha}}{\partial\hat{y}_3}+\widehat{C}_{14}\frac{\partial\widehat{N}_3^{\alpha}}{\partial\hat{y}_2^*}+\widehat{C}_{13}\frac{\partial\widehat{N}_3^{\alpha}}{\partial\hat{y}_3}\right\rangle,\\\widehat{C}_{2\alpha}^{\mathrm{NCP}}&=\left\langle\widehat{C}_{2\alpha}+\widehat{C}_{22}\frac{\partial\widehat{N}_2^{\alpha}}{\partial\hat{y}_2^*}+\widehat{C}_{24}\frac{\partial\widehat{N}_2^{\alpha}}{\partial\hat{y}_3}+\widehat{C}_{24}\frac{\partial\widehat{N}_3^{\alpha}}{\partial\hat{y}_2^*}+\widehat{C}_{23}\frac{\partial\widehat{N}_3^{\alpha}}{\partial\hat{y}_3}\right\rangle,\\\widehat{C}_{3\alpha}^{\mathrm{NCP}}&=\left\langle\widehat{C}_{3\alpha}+\widehat{C}_{23}\frac{\partial\widehat{N}_2^{\alpha}}{\partial\hat{y}_2^*}+\widehat{C}_{34}\frac{\partial\widehat{N}_2^{\alpha}}{\partial\hat{y}_3}+\widehat{C}_{34}\frac{\partial\widehat{N}_3^{\alpha}}{\partial\hat{y}_2^*}+\widehat{C}_{33}\frac{\partial\widehat{N}_3^{\alpha}}{\partial\hat{y}_3}\right\rangle,\\\widehat{C}_{4\alpha}^{\mathrm{NCP}}&=\left\langle\widehat{C}_{4\alpha}+\widehat{C}_{24}\frac{\partial\widehat{N}_2^{\alpha}}{\partial\hat{y}_2^*}+\widehat{C}_{44}\frac{\partial\widehat{N}_2^{\alpha}}{\partial\hat{y}_3}+\widehat{C}_{44}\frac{\partial\widehat{N}_3^{\alpha}}{\partial\hat{y}_2^*}+\widehat{C}_{34}\frac{\partial\widehat{N}_3^{\alpha}}{\partial\hat{y}_3}\right\rangle,\\\widehat{C}_{5\alpha}^{\mathrm{NCP}}&=\left\langle\widehat{C}_{5\alpha}+\widehat{C}_{56}\frac{\partial\widehat{N}_1^{\alpha}}{\partial\hat{y}_2^*}+\widehat{C}_{55}\frac{\partial\widehat{N}_1^{\alpha}}{\partial\hat{y}_3}\right\rangle,\\\widehat{C}_{6\alpha}^{\mathrm{NCP}}&=\left\langle\widehat{C}_{6\alpha}+\widehat{C}_{66}\frac{\partial\widehat{N}_1^{\alpha}}{\partial\hat{y}_2^*}+\widehat{C}_{56}\frac{\partial\widehat{N}_1^{\alpha}}{\partial\hat{y}_3}\right\rangle.\end{aligned} \tag{31}$$

A useful characteristic of the AEH method is that it provides information about the micro-stresses and micro-strains. Using the obtained effective properties of the NCP, the mesoscale problem (that will be described later) can be solved and the meso-strains $\hat{\varepsilon}_{mn}^{(0*)}$ can be computed. Then the micro-stresses and micro-strains are obtained from the solution of the unit cell problem (21), using the equations

$$\hat{\sigma}_{ij}^{(0)}=\left(\widehat{C}_{ijmn}+\widehat{C}_{ijkl}\overline{\mathcal{L}}_k\widehat{N}_l^{mn}\right)\hat{\varepsilon}_{mn}^{(0*)}, \tag{32}$$

$$\hat{\varepsilon}_{ij}^{(0)}=\hat{\varepsilon}_{ij}^{(0*)}+\frac{1}{2}\left(\overline{\mathcal{L}}_i\widehat{N}_j^{mn}+\overline{\mathcal{L}}_j\widehat{N}_i^{mn}\right)\hat{\varepsilon}_{mn}^{(0*)}. \tag{33}$$

## 4. Effective properties of the "fuzzy fiber" composite

Having defined the effective properties of the NCP, the homogenization of the actual composite can be determined using again the AEH method. The actual composite can be described easier in Cartesian coordinates, which necessitates to transfer the effective properties of the NCP from cylindrical $(r,\theta,z)$ to Cartesian $(x_1,x_2,x_3)$ coordinates. The obtained NCP effective properties can be transformed from a cylindrical coordinates form $\widehat{C}^{\mathrm{NCP}}$ to a Cartesian coordinates form $C^{\mathrm{NCP}}$ according to the rotation formula for fourth order tensors

$$C_{ijkl}^{\mathrm{NCP}}=R_{im}R_{jn}R_{ko}R_{lp}\widehat{C}_{mnop}^{\mathrm{NCP}} \tag{34}$$

with

$$\mathbf{R}=\begin{pmatrix}\cos\theta & -\sin\theta & 0\\ \sin\theta & \cos\theta & 0\\ 0 & 0 & 1\end{pmatrix}. \tag{35}$$

Here we need to mention that, according to the analysis of the previous section, the effective coefficients $\widehat{C}_{ijkl}^{\mathrm{NCP}}$ of the NCP are functions of the radius $r$. In Cartesian coordinates, we have $r^2=x_1^2+x_2^2$. Using the Voigt notation, the stiffness tensor of the NCP is given in Cartesian coordinates by

$$\mathbf{C}^{\mathrm{NCP}}=\begin{pmatrix}C_{11}^{\mathrm{NCP}} & C_{12}^{\mathrm{NCP}} & C_{13}^{\mathrm{NCP}} & 0 & 0 & C_{16}^{\mathrm{NCP}}\\ C_{12}^{\mathrm{NCP}} & C_{22}^{\mathrm{NCP}} & C_{23}^{\mathrm{NCP}} & 0 & 0 & C_{26}^{\mathrm{NCP}}\\ C_{13}^{\mathrm{NCP}} & C_{23}^{\mathrm{NCP}} & C_{33}^{\mathrm{NCP}} & 0 & 0 & C_{36}^{\mathrm{NCP}}\\ 0 & 0 & 0 & C_{44}^{\mathrm{NCP}} & C_{45}^{\mathrm{NCP}} & 0\\ 0 & 0 & 0 & C_{45}^{\mathrm{NCP}} & C_{55}^{\mathrm{NCP}} & 0\\ C_{16}^{\mathrm{NCP}} & C_{26}^{\mathrm{NCP}} & C_{36}^{\mathrm{NCP}} & 0 & 0 & C_{66}^{\mathrm{NCP}}\end{pmatrix}, \tag{36}$$

where

$$C_{11}^{\mathrm{NCP}}=\frac{\widehat{C}_{11}^{\mathrm{NCP}}x_1^4+2\left(\widehat{C}_{12}^{\mathrm{NCP}}+2\widehat{C}_{66}^{\mathrm{NCP}}\right)x_1^2x_2^2+\widehat{C}_{22}^{\mathrm{NCP}}x_2^4}{\left(x_1^2+x_2^2\right)^2},$$

$$C_{12}^{\mathrm{NCP}}=\frac{\widehat{C}_{12}^{\mathrm{NCP}}\left(x_1^4+x_2^4\right)+\left(\widehat{C}_{11}^{\mathrm{NCP}}+\widehat{C}_{22}^{\mathrm{NCP}}-4\widehat{C}_{66}^{\mathrm{NCP}}\right)x_1^2x_2^2}{\left(x_1^2+x_2^2\right)^2},$$

$$C_{13}^{\mathrm{NCP}}=\frac{\widehat{C}_{13}^{\mathrm{NCP}}x_1^2+\widehat{C}_{23}^{\mathrm{NCP}}x_2^2}{x_1^2+x_2^2},$$

$$C_{16}^{\mathrm{NCP}}=\frac{(\widehat{C}_{11}^{\mathrm{NCP}}-\widehat{C}_{12}^{\mathrm{NCP}}-2\widehat{C}_{66}^{\mathrm{NCP}})x_1^3x_2+\left(\widehat{C}_{12}^{\mathrm{NCP}}-\widehat{C}_{22}^{\mathrm{NCP}}+2\widehat{C}_{66}^{\mathrm{NCP}}\right)x_1x_2^3}{\left(x_1^2+x_2^2\right)^2},$$

$$C_{22}^{\mathrm{NCP}}=\frac{\widehat{C}_{11}^{\mathrm{NCP}}x_2^4+2\left(\widehat{C}_{12}^{\mathrm{NCP}}+2\widehat{C}_{66}^{\mathrm{NCP}}\right)x_1^2x_2^2+\widehat{C}_{22}^{\mathrm{NCP}}x_1^4}{\left(x_1^2+x_2^2\right)^2},$$

$$C_{23}^{\mathrm{NCP}}=\frac{\widehat{C}_{13}^{\mathrm{NCP}}x_2^2+\widehat{C}_{23}^{\mathrm{NCP}}x_1^2}{x_1^2+x_2^2},$$

$$C_{26}^{\mathrm{NCP}}=\frac{\left(\widehat{C}_{11}^{\mathrm{NCP}}-\widehat{C}_{12}^{\mathrm{NCP}}-2\widehat{C}_{66}^{\mathrm{NCP}}\right)x_1x_2^3+\left(\widehat{C}_{12}^{\mathrm{NCP}}-\widehat{C}_{22}^{\mathrm{NCP}}+2\widehat{C}_{66}^{\mathrm{NCP}}\right)x_1^3x_2}{\left(x_1^2+x_2^2\right)^2},$$

$$C_{33}^{\mathrm{NCP}}=\widehat{C}_{33}^{\mathrm{NCP}},$$

$$C_{36}^{\mathrm{NCP}}=\frac{(\widehat{C}_{13}^{\mathrm{NCP}}-\widehat{C}_{23}^{\mathrm{NCP}})x_1x_2}{x_1^2+x_2^2},$$

$$C_{44}^{\mathrm{NCP}}=\frac{\widehat{C}_{44}^{\mathrm{NCP}}x_1^2+\widehat{C}_{55}^{\mathrm{NCP}}x_2^2}{x_1^2+x_2^2},$$

$$C_{45}^{\mathrm{NCP}}=\frac{\left(\widehat{C}_{55}^{\mathrm{NCP}}-\widehat{C}_{44}^{\mathrm{NCP}}\right)x_1x_2}{x_1^2+x_2^2},$$

$$C_{55}^{\mathrm{NCP}}=\frac{\widehat{C}_{44}^{\mathrm{NCP}}x_2^2+\widehat{C}_{55}^{\mathrm{NCP}}x_1^2}{x_1^2+x_2^2},$$

$$C_{66}^{\mathrm{NCP}}=\frac{\left(\widehat{C}_{11}^{\mathrm{NCP}}-2\widehat{C}_{12}^{\mathrm{NCP}}+\widehat{C}_{22}^{\mathrm{NCP}}\right)x_1^2x_2^2+\widehat{C}_{66}^{\mathrm{NCP}}\left(x_1^2-x_2^2\right)^2}{\left(x_1^2+x_2^2\right)^2}.$$

The other two material components of the composite, the matrix and the carbon fiber, are generally assumed as homogeneous isotropic or transversely isotropic materials, with the axis of symmetry parallel to the axis of the fiber. Under these conditions, the application of the AEH method for the second periodic problem with characteristic length $\epsilon$ (Fig. 2b) follows the standard approach (Sanchez-Palencia, 1978) and is presented in Appendix A.

In the above methodology for obtaining effective properties of "fuzzy fiber" composites we utilize a two step homogenization method, because in the first step (nanocomposite layer) we express our equations in cylindrical coordinates and in the second step (actual composite) we use Cartesian coordinates. A one step homogenization would require everything to be expressed in one coordinate system, e.g., Cartesian, leading to solve a curvilinear unit shell in the microscale level (nanocomposite layer).

## 5. Example

The numerical example presented in this section is motivated by the experiments presented in Sager et al. (2009). T650 carbon fibers with diameter 5 μm are coated with radially aligned hollow carbon nanotubes of 2 μm length. The CNTs have internal radius 0.51 nm, external radius 0.85 nm. The "fuzzy fibers" are embedded in EPIKOTE 862 resin. The intermediate layer contains CNTs with average volume fraction 42.17%. The properties of the CNTs are assumed the same as the properties of the graphene (Seidel and Lagoudas, 2006). The mechanical properties of the carbon fibers, the resin and the CNTs are shown in Table 1.

For the computations we used the finite element program COMSOL Multiphysics. The effective properties for the nanocomposite were obtained for both the tetragonal and the hexagonal arrangement of the CNTs. Since the periodic structure of the nanocomposite depends on the radius, we needed to solve numerically several unit cells. Each unit cell represents a different profile of the nanocomposite with respect to radius and the volume fraction of the CNTs decreases as the radius increases. Figs. 4 and 5 show several unit cells that were solved for tetragonal and hexagonal arrangement of the CNTs respectively. Here the arrangement of CNTs is exactly tetragonal or hexagonal only at the interphase between the carbon fiber and the nanocomposite. As we move closer to the matrix, the length of the unit cell at the $r\bar{\theta}$ direction elongates, disturbing the tetragonal or hexagonal symmetry.

Since the homogenization problem reduces to 2D problem, we use 2D mesh, which differs for each microscale unit cell. Details of the 2D FE meshing for two unit cells of the nanocomposite with hexagonal arrangement of CNTs are presented in Fig. 6. The periodicity boundary condition is imposed by applying the same $\widehat{N}_i^{mn}$ on opposite sides of the unit cells. For the purposes of the numerical analysis, we use quadratic Lagrange finite elements.

The obtained effective properties are shown in Figs. 7 and 8. As it can be seen from these figures, the NCP becomes more cylindrically

**Table 1**
Mechanical properties of layers.

| | |
|---|---|
| *T650 Carbon fiber* (CYTEC, 2011) | |
| Axial Young's modulus | 241 GPa |
| Transverse Young's modulus | 14.5 GPa |
| Axial shear modulus | 22.8 GPa |
| Transverse shear modulus | 4.8 GPa |
| Axial Poisson's ratio | 0.27 |
| *EPIKOTE 862 resin* | |
| Young's modulus | 3 GPa |
| Poisson's ratio | 0.3 |
| *CNT* | |
| Young's modulus | 1100 GPa |
| Poisson's ratio | 0.14 |

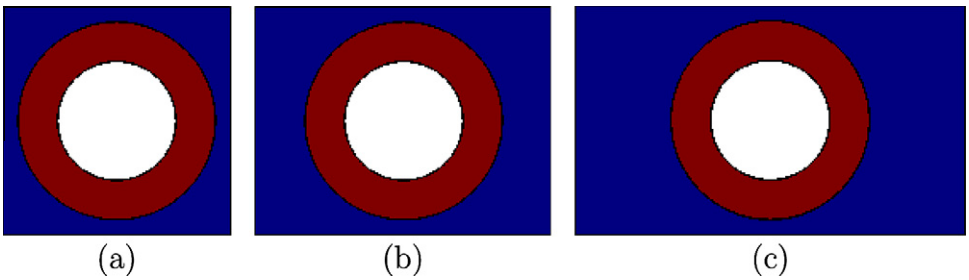


**Fig. 4.** Unit cell of the NCP for $r$ equal to (a) 2.5 μm, (b) 3.25 μm and (c) 4.25 μm. Tetragonal arrangement.

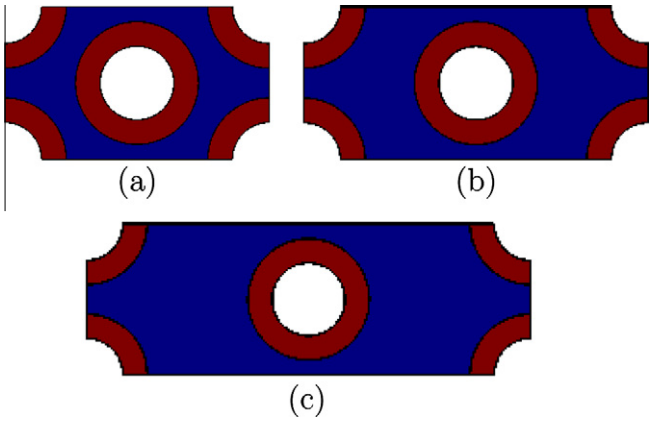


**Fig. 5.** Unit cell of the NCP for $r$ equal to (a) 2.5 μm, (b) 3.25 μm and (c) 4.25 μm. Hexagonal arrangement.

orthotropic with the increase of radius. The radial Young's modulus $E_{rr}$ and the transverse shear modulus $G_{r\theta}$ present the largest reduction moving from the carbon fiber to the matrix: 44.1% and 58.5%, respectively for the tetragonal arrangement and 44.1% and 54.2%, respectively for the hexagonal arrangement. For the hexagonal arrangement the NCP in cylindrically transversely isotropic only at the interphase between NCP and carbon fiber ($r$ = 2.5 μm). Moreover the tetragonal arrangement favors the orthotropy more than the hexagonal arrangement. At the interphase between NCP and epoxy resin the difference between the transverse Young's moduli $E_{\theta\theta}$ and $E_{zz}$ is 31.4% and 20.6% for the tetragonal and hexagonal CNT arrangement respectively. At the same interphase the difference between the transverse shear moduli $G_{rz}$ and $E_{r\theta}$ is 38.9% and 27.4% for the tetragonal and hexagonal CNT arrangement respectively. From the results it is clear that all the effective properties of the NCP are strongly affected by the radius. This radial dependency can be simulated by assuming that all the mechanical properties can be described with fifth order polynomials with respect to radius.

In the second step of the homogenization, the NCP is substituted by the effective medium, which is introduced in the mesoscale unit cell. The program we used for the numerical results is again the COMSOL Multiphysics software, and we used a 2D mesh, details of which are shown in Fig. 9b. The periodicity in the unit cell is imposed by applying the same $N_i^{mn}$ on opposite sides of the hexagon. For the purposes of the numerical analysis, we use quadratic Lagrange finite elements. The spatially variable homogenized moduli of the nanocomposite are introduced in COMSOL as fifth order polynomials.

As it can be seen in Fig. 10, transferring the effective properties from the cylindrical to Cartesian coordinates, produces a fully anisotropic behavior for the NCP. Terms like $C_{16}$ are no longer zero, only the average $C_{16}$ over the whole NCP becomes zero. For the numerical example we use a volume fraction of 60% for the "fuzzy fiber" (carbon fiber plus NCP) inside the resin. The numerically obtained effective properties (Table 2) show that the arrangement of the CNTs in the NCP do not alter significantly the behavior of the actual composite. In both arrangements (tetragonal and hexagonal) the overall behavior of the "fuzzy fiber" composite is transversely isotropic with axis of symmetry the axis of the carbon fiber. This transverse isotropy is observed in typical fiber composites, indicating that the presence of the NCP changes the mechanical performance but not the level of anisotropy of the actual composite.

In Table 2 we also present the results from an analytical approach. In this approach the nanocomposite layer is assumed to behave as a classical unidirectional composite, which is a transversely isotropic medium with the axis of symmetry parallel to the axis of CNTs (i.e., in the radial direction of the carbon fiber). Its effective behavior can be obtained using standard micromechanics techniques, like Mori–Tanaka. Having obtained the nanocomposite properties, the "fuzzy fiber" composite effective behavior is determined using an extension of the composite cylinder method. The five independent effective properties in the case of a regular fiber composite are obtained by solving five appropriate boundary value

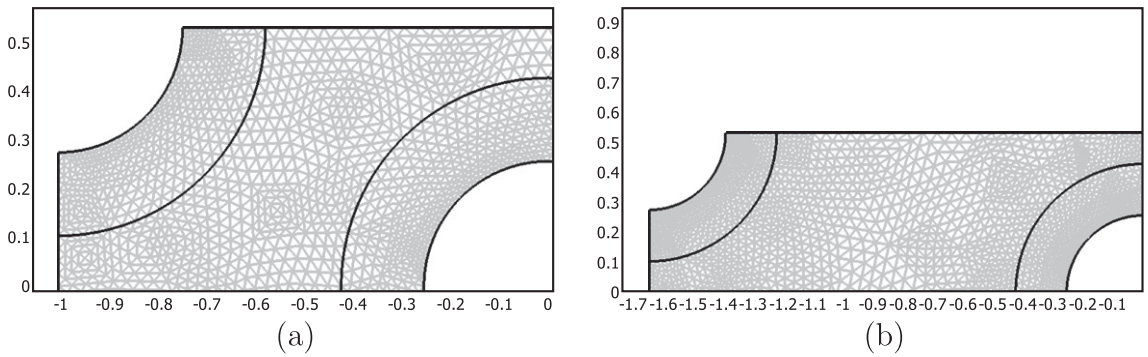


**Fig. 6.** Part of the finite element mesh of microscale unit cells with $r$ equal to (a) 2.5 μm (9120 triangular elements total) and (b) 4.5 μm (11,104 triangular elements total). Hexagonal arrangement.

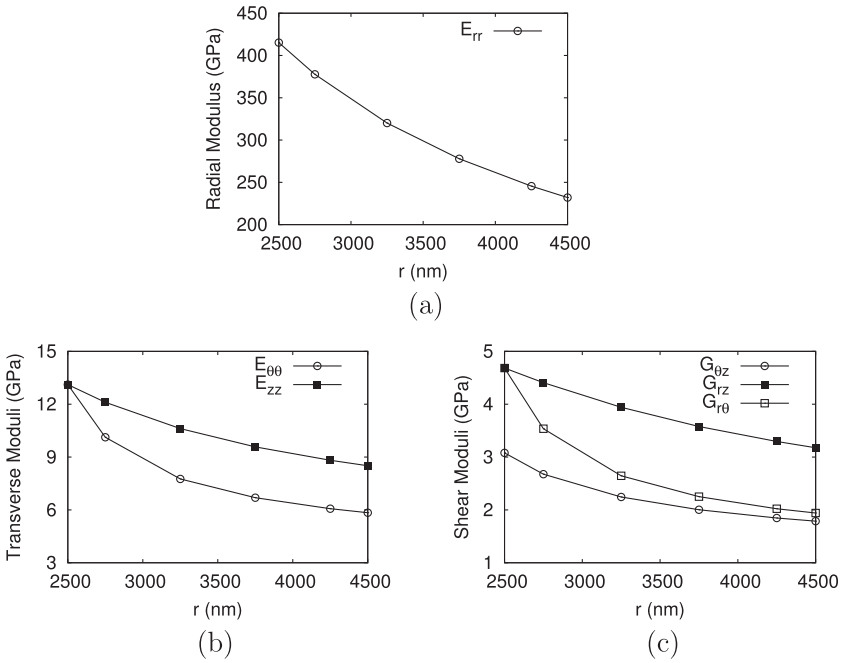


**Fig. 7.** Effective properties of NCP for tetragonal arrangement of CNTs.

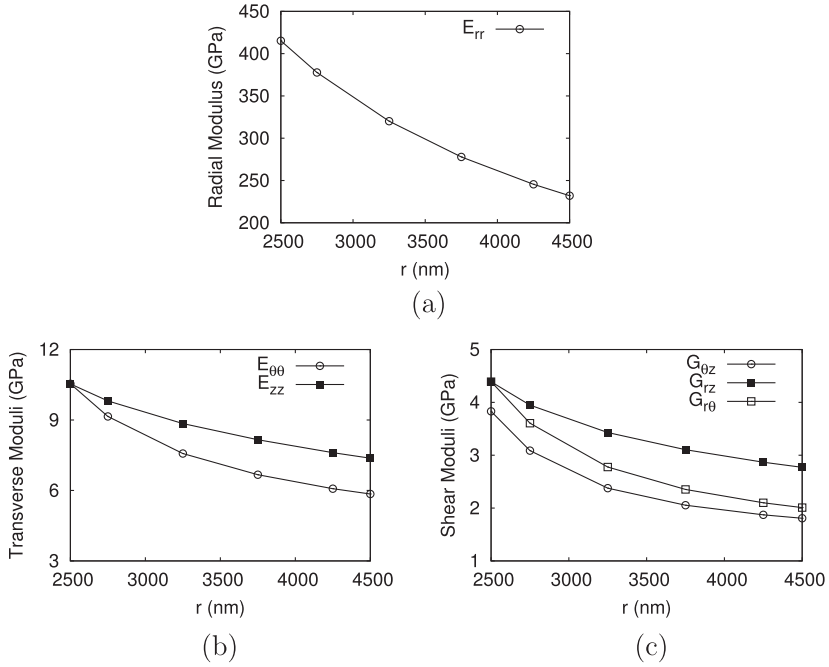


**Fig. 8.** Effective properties of NCP for hexagonal arrangement of CNTs.

problems: the four problems for determining the axial Young's Modulus, the axial Poison's ratio, the axial shear modulus and the transverse bulk modulus are described in Hashin and Rosen (1964). The fifth problem, from which we compute the transverse shear modulus, is described in the Christensen's three-phase model (Christensen and Lo, 1979; Christensen, 1979). For multi-walled CNT composites, the effective properties can be obtained by the methodology proposed in Seidel and Lagoudas (2006). Chatzigeorgiou et al. (2011) extend (Seidel and Lagoudas, 2006) methodology, studying the case of the "fuzzy fiber" composite, where the nanocomposite behaves as an orthotropic layer. Suitable displacement fields for the five boundary value problems are presented and the effective properties of the "fuzzy fiber" composite are obtained.

As it is shown in Table 2, the results from the analytical micromechanics approach are very close to the effective properties of "fuzzy fiber" composites with hexagonal CNTs arrangement. The results indicate that the transverse shear modulus of the composite has approximately 100% enhancement compared to the matrix shear modulus (1.15 GPa). This increase will be reduced if we consider the reduction of the carbon fiber mechanical properties due to the coating procedure (Sager et al., 2009).

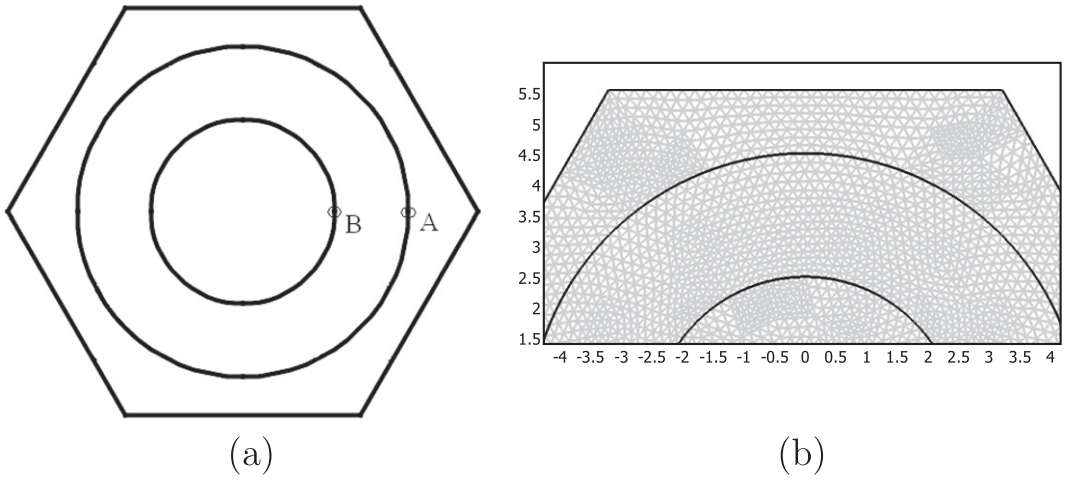


**Fig. 9.** (a) Geometry and (b) part of the finite element mesh of mesoscale unit cell (10,080 triangular elements total).

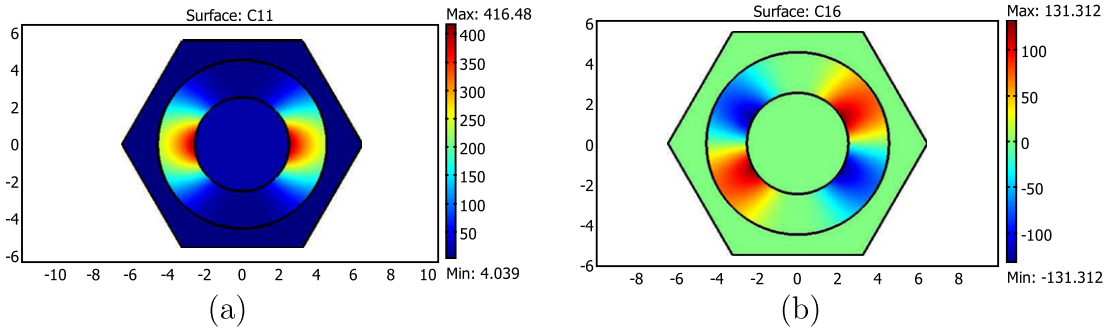


**Fig. 10.** Distribution of the stiffness coefficients (a) $C_{11}$ and (b) $C_{16}$ in the mesoscale unit cell. The units are GPa.

The homogenization procedure described in the previous sections provides information about local stresses and strains in both mesoscale and microscale level. In the microscale level, the computation of the micro-stresses that appear in the nanocomposite are of great importance. The local stress fields that appear between the carbon fiber and the CNTs, as well as the matrix and the CNTs significantly influence the interfacial shear strength of the composite. The knowledge of the distribution of the micro-stresses allows also the identification of possible failure modes of the interfacial layer. Lekhnitskii (1977, 1981) studied in his monograph the effect of the local stress field disturbance, due to the materials architecture, on the interfacial strength. Local stresses in CNT composites have been studied both experimentally, using Raman spectroscopy (Zhao and Wagner, 2004), and theoretically with analytical models (Lau, 2003, 2005) and numerical approaches (Liu and Chen, 2003b).

In this example we will present distribution of the micro-stresses in the nanocomposite layer, when the actual composite is subjected to uniform macro-strain $\varepsilon_{xx} = \varepsilon_{11} = 0.5\%$.

**Table 2**
Effective properties of "fuzzy fiber" composites.

| CNTs arrangement in NCP | Axial Young's modulus (GPa) | Transverse Young's modulus (GPa) | Axial shear modulus (GPa) | Transverse shear modulus (GPa) | Transverse shear modulus (GPa) |
|---|---|---|---|---|---|
| Tetragonal | 50.10 | 6.89 | 2.65 | 2.38 | 6.40 |
| Hexagonal | 49.45 | 6.92 | 2.55 | 2.39 | 6.40 |
| Analytical | 48.87 | 7.05 | 2.43 | 2.46 | 6.38 |

Using Eq. (A-15) the local strains in the mesoscale unit cell are computed with respect to Cartesian coordinate system and they are presented in Fig. 11. The only non-zero components of the meso-strain tensor are the $\varepsilon_{11}^{(0)}$, $\varepsilon_{12}^{(0)}$, $\varepsilon_{22}^{(0)}$. At the specific points A and B of the mesoscale unit cell (Fig. 9a) the meso-strains are equal to

$$\hat{\varepsilon}_{11}^{(0*)} = \varepsilon_{11}^{(0)} = 5.57 \cdot 10^{-3}, \quad \hat{\varepsilon}_{12}^{(0*)} = \varepsilon_{12}^{(0)} = 1.12 \cdot 10^{-6},$$

$$\hat{\varepsilon}_{22}^{(0*)} = \varepsilon_{22}^{(0)} = -3.97 \cdot 10^{-4}, \quad \text{for point A},$$

$$\hat{\varepsilon}_{11}^{(0*)} = \varepsilon_{11}^{(0)} = 1.52 \cdot 10^{-3}, \quad \hat{\varepsilon}_{12}^{(0*)} = \varepsilon_{12}^{(0)} = -3.99 \cdot 10^{-7},$$

$$\hat{\varepsilon}_{22}^{(0*)} = \varepsilon_{22}^{(0)} = 1.15 \cdot 10^{-3}, \quad \text{for point B}.$$

These values indicate that closer to the carbon fiber the nanocomposite has lower radial strain and higher hoop strain than close to the matrix phase.

In order to represent the micro-stresses in the nanocomposite, the microscale unit cells at the mesoscale points A and B are solved. The micro-stresses are computed from Eq. (32) and their distribution in the corresponding unit cells are presented in Fig. 12. The radial stress on the CNTs close to the epoxy resin (point A) reach the value of 6100 MPa, while close to the carbon fiber (point B) the radial stress is much lower and becomes approximately 1700 MPa. On the other hand, the local hoop stresses on the CNTs reach higher values close to the carbon fiber (145 MPa) than close to the epoxy resin (55 MPa).

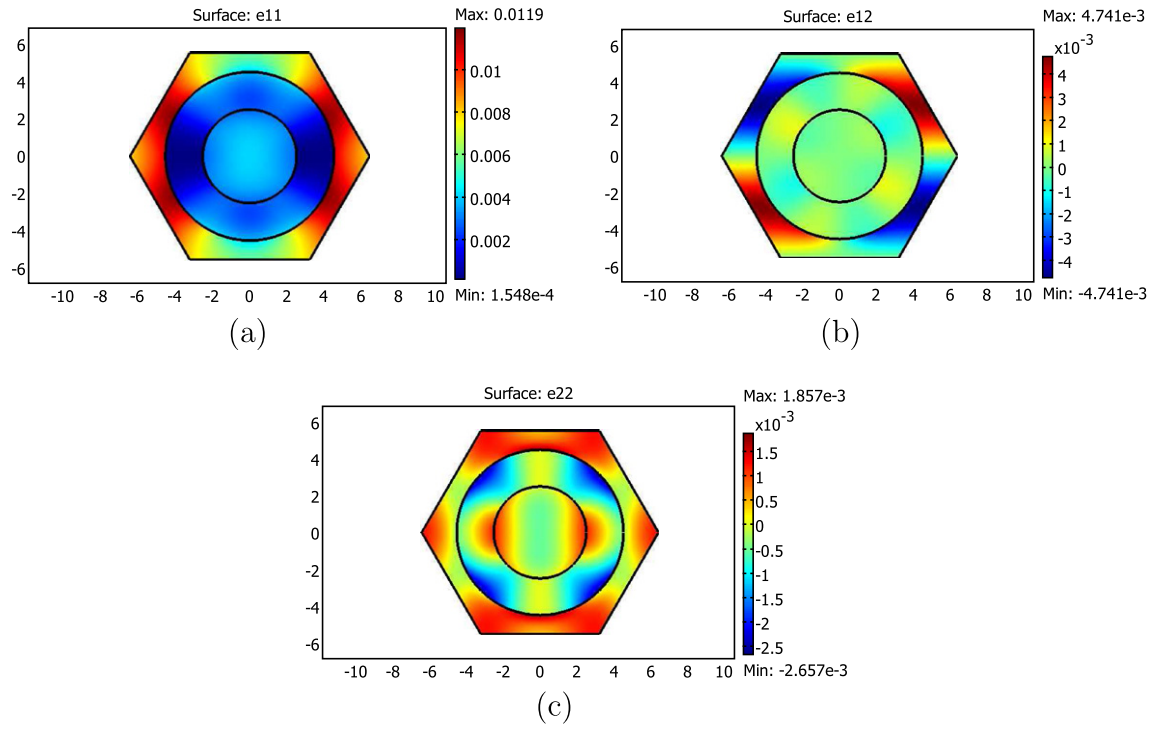


**Fig. 11.** Distribution of meso-strains (a) $\varepsilon_{11}^{(0)}$, (b) $\varepsilon_{12}^{(0)}$ and (c) $\varepsilon_{22}^{(0)}$.

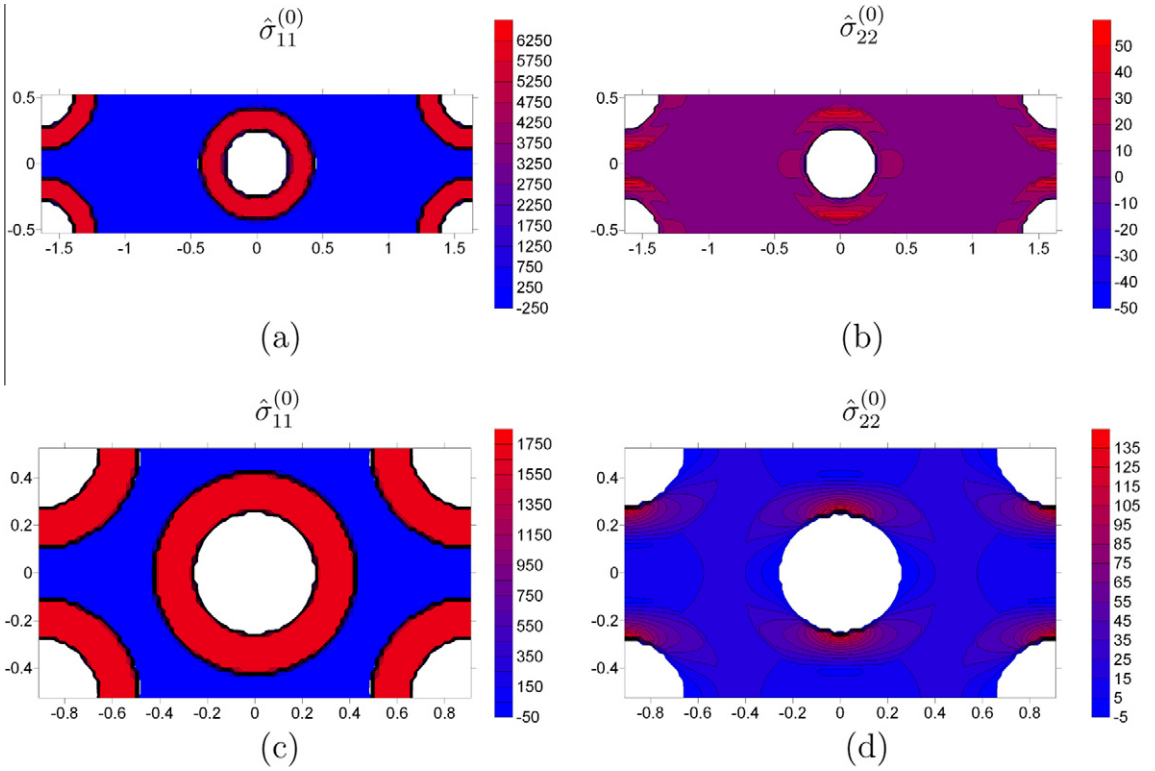


**Fig. 12.** Distribution of micro-stresses at points A and B of the mesoscale unit cell: (a) radial stresses in point A, (b) hoop stresses in point A, (c) radial stresses in point B and (d) hoop stresses in point B. Hexagonal arrangement.

## 6. Conclusions

In this paper we presented a two step homogenization approach, based on the asymptotic expansion homogenization method, in order to evaluate the effective properties of carbon fiber composites, in which the carbon fibers are coated with radially aligned carbon nanotubes (CNTs). From the theoretical analysis it is shown that the homogenization process can be split in two parts, in each

one of which different coordinate system can be used. In each part we can compute local stress and strain fields, allowing to determine micro-stresses in the nanocomposite layer between the carbon fiber and the matrix. In the first part of homogenization, the nanocomposite layer which includes CNTs and matrix show cylindrically orthotropic behavior and the material properties depend on the radius. The results from the second step of homogenization, which includes the mesoscale unit cell, indicate that the nanocomposite does not influence the overall anisotropy of the composite. Additionally the arrangement of CNTs in the nanocomposite (tetragonal and hexagonal) does not change significantly the overall behavior of the "fuzzy fiber" composite. Under uniform macro-strain we observe that the interphase between the carbon fiber and the nanocomposite present lower radial and higher hoop micro-stresses than the interphase between the nanocomposite and the epoxy matrix.

## Acknowledgements

The authors would like to acknowledge the financial support provided by NSF, Grant Nos. DMR-0844082 (IIMEC project) and NSF DMS 0811180. This publication is partially supported by Award No. KUS-C1-016-04, made by King Abdullah University of Science and Technology (KAUST).

## Appendix A. Asymptotic expansion homogenization method in Cartesian coordinates

The equations that describe the behavior of the constituents are the equilibrium equations (neglecting body forces)

$$\frac{\partial \sigma_{ij}^{\epsilon}}{\partial x_j^{\epsilon}} = 0, \tag{A-1}$$

the constitutive law

$$\sigma_{ij}^{\epsilon} = C_{ijkl}^{\epsilon} \frac{\partial u_k^{\epsilon}}{\partial x_l^{\epsilon}}, \tag{A-2}$$

and appropriate boundary conditions. The stiffness tensor in the mesoscale level is a periodic function of $\frac{x_1}{\epsilon}$ and $\frac{x_2}{\epsilon}$,

$$C_{ijkl}^{\epsilon} = C_{ijkl}^{\epsilon}\left(\frac{x_1}{\epsilon}, \frac{x_2}{\epsilon}\right) = C_{ijkl}(y_1, y_2). \tag{A-3}$$

Expanding the displacements in terms of the mesoscale characteristic length $\epsilon$,

$$u_i^{\epsilon} = u_i^{(0)}(x_1, x_2, x_3) + \epsilon u_i^{(1)}(x_1, x_2, x_3, y_1, y_2) + \epsilon^2 u_i^{(2)}(x_1, x_2, x_3, y_1, y_2) + \cdots \tag{A-4}$$

and substituting in Eqs. (A-2) and (A-1) we get an expanded form of the equilibrium equations, in which the $\epsilon^{-1}$ terms (meso-equations) are written

$$-\frac{\partial}{\partial y_j}\left(C_{ijkl}\frac{\partial u_k^{(1)}}{\partial y_l}\right) = \frac{\partial u_k^{(0)}}{\partial x_l}\frac{\partial C_{ijkl}}{\partial y_j}. \tag{A-5}$$

Considering $u_k^{(0)}$ as known, we assume that $u_i^{(1)}$ is given, up to an additive function on $x_1$, $x_2$, $x_3$, from

$$u_i^{(1)} = N_i^{mn}\frac{\partial u_m^{(0)}}{\partial x_n}, \tag{A-6}$$

where $N_i^{mn}$ is given from the auxiliary system

$$\frac{\partial}{\partial y_j}\left(C_{ijkl}\frac{\partial N_k^{mn}}{\partial y_l} + C_{ijmn}\right) = 0. \tag{A-7}$$

Returning to the equilibrium equations and the $\epsilon^0$ terms, we can easily show that the macro-equations in terms of the meso-stresses $\sigma_{ij}^{(0)}$ are written

$$\frac{\partial \langle \sigma_{ij}^{(0)} \rangle}{\partial x_j^{\epsilon}} = 0 \tag{A-8}$$

and the effective properties of the actual composite are given by

$$C_{ijkl}^{\text{eff}} = \left\langle\left\langle C_{ijkl} + C_{ijmn}\frac{\partial N_m^{kl}}{\partial y_n}\right\rangle\right\rangle, \tag{A-9}$$

where

$$\langle\langle \phi \rangle\rangle = \frac{1}{V^{mes}}\int_{-y_1'/2}^{y_1'/2}\int_{-y_2'/2}^{y_2'/2}\int_{-y_3'/2}^{y_3'/2}\phi(y_1, y_2, y_3)\mathrm{d}y_1\,\mathrm{d}y_2\,\mathrm{d}y_3 \tag{A-10}$$

and $V^{mes}$ is the volume in the mesoscale level.

In the case of our composite, the meso-macroscale structure does not vary with $y_3$ (monoclinic materials) and the derivatives with respect to $y_3$ vanish. This leads, with the help of the Voigt notation, to the meso-equations

$$\begin{aligned}&-\frac{\partial}{\partial y_1}\left(C_{11}\frac{\partial N_1^{\alpha}}{\partial y_1} + C_{16}\frac{\partial N_1^{\alpha}}{\partial y_2} + C_{16}\frac{\partial N_2^{\alpha}}{\partial y_1} + C_{12}\frac{\partial N_2^{\alpha}}{\partial y_2}\right)\\ &-\frac{\partial}{\partial y_2}\left(C_{16}\frac{\partial N_1^{\alpha}}{\partial y_1} + C_{66}\frac{\partial N_1^{\alpha}}{\partial y_2} + C_{66}\frac{\partial N_2^{\alpha}}{\partial y_1} + C_{26}\frac{\partial N_2^{\alpha}}{\partial y_2}\right)\\ &= \frac{\partial C_{1\alpha}}{\partial y_1} + \frac{\partial C_{6\alpha}}{\partial y_2},\end{aligned} \tag{A-11}$$

$$\begin{aligned}&-\frac{\partial}{\partial y_1}\left(C_{16}\frac{\partial N_1^{\alpha}}{\partial y_1} + C_{66}\frac{\partial N_1^{\alpha}}{\partial y_2} + C_{66}\frac{\partial N_2^{\alpha}}{\partial y_1} + C_{26}\frac{\partial N_2^{\alpha}}{\partial y_2}\right)\\ &-\frac{\partial}{\partial y_2}\left(C_{12}\frac{\partial N_1^{\alpha}}{\partial y_1} + C_{26}\frac{\partial N_1^{\alpha}}{\partial y_2} + C_{26}\frac{\partial N_2^{\alpha}}{\partial y_1} + C_{22}\frac{\partial N_2^{\alpha}}{\partial y_2}\right)\\ &= \frac{\partial C_{6\alpha}}{\partial y_1} + \frac{\partial C_{2\alpha}}{\partial y_2},\end{aligned} \tag{A-12}$$

for $\alpha = 1,2,3,6$ (plane strain problems) and

$$\begin{aligned}&-\frac{\partial}{\partial y_1}\left(C_{55}\frac{\partial N_3^{\alpha}}{\partial y_1} + C_{45}\frac{\partial N_3^{\alpha}}{\partial y_2}\right) - \frac{\partial}{\partial y_2}\left(C_{45}\frac{\partial N_3^{\alpha}}{\partial y_1} + C_{44}\frac{\partial N_3^{\alpha}}{\partial y_2}\right)\\ &= \frac{\partial C_{5\alpha}}{\partial y_1} + \frac{\partial C_{4\alpha}}{\partial y_2},\end{aligned} \tag{A-13}$$

for $\alpha = 4,5$ (anti-plane strain problems). The effective properties are given by

$$C_{1\alpha}^{\text{eff}} = \left\langle\left\langle C_{1\alpha} + C_{11}\frac{\partial N_1^{\alpha}}{\partial y_1} + C_{16}\frac{\partial N_1^{\alpha}}{\partial y_2} + C_{16}\frac{\partial N_2^{\alpha}}{\partial y_1} + C_{12}\frac{\partial N_2^{\alpha}}{\partial y_2}\right\rangle\right\rangle,$$

$$C_{2\alpha}^{\text{eff}} = \left\langle\left\langle C_{2\alpha} + C_{12}\frac{\partial N_1^{\alpha}}{\partial y_1} + C_{26}\frac{\partial N_1^{\alpha}}{\partial y_2} + C_{26}\frac{\partial N_2^{\alpha}}{\partial y_1} + C_{22}\frac{\partial N_2^{\alpha}}{\partial y_2}\right\rangle\right\rangle,$$

$$C_{3\alpha}^{\text{eff}} = \left\langle\left\langle C_{3\alpha} + C_{13}\frac{\partial N_1^{\alpha}}{\partial y_1} + C_{36}\frac{\partial N_1^{\alpha}}{\partial y_2} + C_{36}\frac{\partial N_2^{\alpha}}{\partial y_1} + C_{23}\frac{\partial N_2^{\alpha}}{\partial y_2}\right\rangle\right\rangle,$$

$$C_{6\alpha}^{\text{eff}} = \left\langle\left\langle C_{6\alpha} + C_{16}\frac{\partial N_1^{\alpha}}{\partial y_1} + C_{66}\frac{\partial N_1^{\alpha}}{\partial y_2} + C_{66}\frac{\partial N_2^{\alpha}}{\partial y_1} + C_{26}\frac{\partial N_2^{\alpha}}{\partial y_2}\right\rangle\right\rangle,$$

for $\alpha = 1,2,3,6$ and

$$C_{4\alpha}^{\text{eff}} = \left\langle\left\langle C_{4\alpha} + C_{45}\frac{\partial N_3^{\alpha}}{\partial y_1} + C_{44}\frac{\partial N_3^{\alpha}}{\partial y_2}\right\rangle\right\rangle,$$

$$C_{5\alpha}^{\text{eff}} = \left\langle \left\langle C_{5\alpha} + C_{55}\frac{\partial N_3^{\alpha}}{\partial y_1} + C_{45}\frac{\partial N_3^{\alpha}}{\partial y_2} \right\rangle \right\rangle,$$

for $\alpha = 4,5$.

Using the obtained effective properties of the composite, the macro-Eq. (A-8) are solved for a specific boundary value problem and the terms $\partial u_i^{(0)}/\partial x_j$ are obtained. Then the solution of the unit cell problem (A-7) allows the computation of the meso-stresses and meso-strains in cartesian coordinates, using the equations

$$\sigma_{ij}^{(0)} = \left( C_{ijkl} + C_{ijmn}\frac{\partial N_m^{kl}}{\partial y_n} \right)\frac{\partial u_k^{(0)}}{\partial x_l}, \tag{A-14}$$

$$\varepsilon_{ij}^{(0)} = \frac{1}{2}\left( \frac{\partial u_i^{(0)}}{\partial x_j} + \frac{\partial u_j^{(0)}}{\partial x_i} \right) + \frac{1}{2}\left( \frac{\partial N_i^{kl}}{\partial y_j} + \frac{\partial N_j^{kl}}{\partial y_i} \right)\frac{\partial u_k^{(0)}}{\partial x_l}. \tag{A-15}$$

The meso-strains $\hat{\varepsilon}_{ij}^{(0*)}$ in cylindrical coordinates are given from (A-15) with proper rotation of the system from Cartesian to cylindrical coordinates.

## References


Awasthi, A.P., Lagoudas, D.C., Hammerand, D.C., 2009. Modeling of graphene-polymer interfacial mechanical behavior using molecular dynamics. Modelling and Simulation in Materials Science and Engineering 17 (1), 015002.

Bensoussan, A., Lions, J., Papanicolaou, G., 1978. Asymptotic Methods for Periodic Structures. North Holland.

Chatterjee, D., 1970. Some problems of plane strain in a non-homogeneous isotropic cylinder. Pure and Applied Geophysics 82 (1), 34–40.

Chatzigeorgiou, G., Charalambakis, N., Murat, F., 2008. Homogenization problems of a hollow cylinder made of elastic materials with discontinuous properties. International Journal of Solids and Structures 45, 5165–5180.

Chatzigeorgiou, G., Seidel, G.D., Lagoudas, D.C., 2011. Effective mechanical properties of "fuzzy fiber" composites. in preparation.

Chen, T., Chung, C.-T., Lin, W.-L., 2000. A revisit of a cylindrically anisotropic tube subjected to pressuring, shearing, torsion, extension and a uniform temperature change. International Journal of Solids and Structures 37, 5143–5159.

Christensen, R.M., 1979. Mechanics of Composite Materials. Dover.

Christensen, R.M., Lo, K., 1979. Solutions for effective shear properties in three phase sphere and cylinder models. Journal of the Mechanics and Physics of Solids 27 (315–330).

Chung, P.W., Tamma, K.K., Namburu, R.R., 2001. Asymptotic expansion homogenization for heterogeneous media: computational issues and applications. Composites: Part A 32, 1291–1301.

CYTEC, 2011. Typical properties for thornel carbon fibers - standard products (bp amoco chemicals). <cytec.com/engineered-materials/downloads/ThornelTP.pdf>.

Efendiev, Y., Hou, T., 2009. Multiscale Finite Element Methods. Theory and Applications. Springer.

Fisher, F.T., Bradshaw, R.D., Brinson, L.C., 2002. Effects of nanotube waviness on the modulus of nanotube-reinforced polymers. Applied Physics Letters 80 (24), 4647–4649.

Fisher, F.T., Bradshaw, R.D., Brinson, L.C., 2003. Fiber waviness in nanotube-reinforced polymer composites. i: modulus predictions using effective nanotube properties. Composites Science and Technology 63 (11), 1689–1703.

Frankland, S., Harik, V., Odegard, G., Brenner, O., Gates, T., 2002. The stress–strain behavior of polymer-nanotube composites from molecular dynamics simulations. Tech. rep., NASA ICASE.

Frankland, S., Harik, V., Odegard, G., Brenner, D., Gates, T., 2003. The stress–strain behavior of polymer-nanotube composites from molecular dynamics simulation. Composites Science and Technology 63, 1655–1661.

Griebel, M., Hamaekers, J., 2004. Molecular dynamics simulations of the elastic moduli of polymer-carbon nanotube composites. Computer Methods in Applied Mechanics and Engineering 193, 1773–1788.

Hadjiev, V.G., Lagoudas, D.C., Oh, E.-S., Thakre, P., Davis, D., Files, B.S., Yowell, L., Arepalli, S., Bahr, J.L., Tour, J.M., 2006. Buckling instabilities of octadecylamine functionalized carbon nanotubes embedded in epoxy. Composites Science and Technology 66, 128–136.

Haque, A., Ramasetty, A., 2005. Theoretical study of stress transfer in carbon nanotube reinforced polymer matrix composites. Composite Structures 71, 68–77.

Hashin, Z., Rosen, B.W., 1964. The elastic moduli of fiber-reinforced materials. Journal of Applied Mechanics 31, 223–232.

Horgan, C., Chan, A., 1999a. The pressurized hollow cylinder or disk problem for functionally graded isotropic linearly elastic materials. Journal of Elasticity 55 (1), 43–59.

Horgan, C., Chan, A., 1999b. The stress response of functionally graded isotropic linearly elastic rotating disks. Journal of Elasticity 55 (1), 219–230.

Hosseini Kordkheili, S., Naghdabadi, R., 2007. Thermoelastic analysis of a functionally graded rotating disk. Composite Structures 79, 508–516.

Iijima, S., 1991. Helical microtubules of graphitic carbon. Nature 354, 56–58.

Kalamkarov, A.L., Kolpakov, A.G., 1997. Analysis, Design and Optimization of Composite Structures. Wiley.

Lau, K., 2003. Interfacial bonding characteristics of nanotube/polymer composites. Chemical Physics Letters 370, 399–405.

Lekhnitskii, S.G., 1977. The Theory of Elasticity of an Anisotropic Body. Nauka, Moscow (in Russian).

Lekhnitskii, S.G., 1981. The Theory of Elasticity of an Anisotropic Body. Mir Publishers (English Translation).

Liu, Y., Chen, X., 2003a. Evaluations of the effective material properties of carbon nanotube-based composites using nanoscale representative volume element. Mechanics of Materials 35, 69–81.

Liu, Y.J., Chen, X.L., 2003b. Continuum models of carbon nanotube-based composites using the boundary element method. Electronic Journal of Boundary Elements 1 (2), 316–335.

Lourie, O., Wagner, H., 1998. Transmission electron microscopy observations of fracture of single-wall carbon nanotubes under axial tension. Applied Physics Letters 73 (24), 3527–3529.

McCarthy, B., Coleman, J., Czerw, R., Dalton, A., in het Panhuis, M., Maiti, A., Drury, A., Bernier, P., Nagy, J., Lahr, B., Byrne, H., Carroll, D., Blau, W., 2002. A microscopic and spectroscopic study of interactions between carbon nanotubes and a conjugated polymer. Journal of Physical Chemistry B 106, 2210–2216.

Milo, S., Shaffer, P., Windle, A.H., 1999. Fabrication and characterization of carbon nanotube/poly(vinyl alcohol) composites. Advanced Materials 11 (11), 937–941.

Nie, G., Batra, R., 2010a. Exact solutions and material tailoring for functionally graded hollow circular cylinders. Journal of Elasticity 99 (2), 179–201.

Nie, G., Batra, R., 2010b. Material tailoring and analysis of functionally graded isotropic and incompressible linear elastic hollow cylinders. Composite Structures 92 (2), 265–274.

Nie, G., Batra, R., 2010c. Static deformations of functionally graded polar-orthotropic cylinders with elliptical inner and circular outer surfaces. Composites Science and Technology 70, 450–457.

Odegard, G., Gates, T., Wise, K., Park, C., Siochi, E., 2003. Constitutive modeling of nanotube-reinforced polymer composites. Composites Science and Technology 63 (11), 1671–1687.

Owhadi, H., Zhang, L., 2007. Metric based up-scaling. Communications on Pure and Applied Mathematics LX, 06750723.

Peigney, A., Laurent, C., Flahaut, E., Rousset, A., 2000. Carbon nanotubes in novel ceramic matrix nanocomposites. Ceramics International 26, 677–683.

Popov, V., 2004. Carbon nanotubes: properties and applications. Materials Science and Engineering R 43, 61–102.

Potschke, P., Bhattacharyya, A.R., Janke, A., 2004. Carbon nanotube-filled polycarbonate composites produced by melt mixing and their use in blends with polyethylene. Carbon 42, 965–969.

Ruhi, M., Angoshtari, A., Naghdabadi, R., 2005. Thermoelastic analysis of thick-walled finite-length cylinders of functionally graded materials. Journal of Thermal Stresses 28, 391–408.

Sager, R.J., Klein, P.J., Lagoudas, D.C., Zhang, Q., Liu, J., Dai, L., Baur, J.W., 2009. Effect of carbon nanotubes on the interfacial shear strength of T650 carbon fiber in an epoxy matrix. Composites Science and Technology 69, 898–904.

Salvetat-Delmotte, J.-P., Rubio, A., 2002. Mechanical properties of carbon nanotubes: a fiber digest for beginners. Carbon 40, 1729–1734.

Sanchez-Palencia, E., 1978. Non-Homogeneous Media and Vibration Theory. Lecture Notes in Physics, vol. 127. Springer-Verlag.

Seidel, G.D., Lagoudas, D.C., 2006. Micromechanical analysis of the effective elastic properties of carbon nanotube reinforced composites. Mechanics of Materials 38, 884–907.

Spanos, P.D., Kontsos, A., 2008. A multiscale Monte Carlo finite element method for determining mechanical properties of polymer nanocomposites. Probabilistic Engineering Mechanics 23 (4), 456–470.

Star, A., Stoddart, J., Steuerman, D., Diehl, M., Boukai, A., Wong, E., 2001. Preparation and properties of polymer-wrapped single-walled carbon nanotubes. Angewandte Chemie International Edition 40 (9), 1721–1725.

Tarn, J.-Q., 2002. Exact solutions of a piezoelectric circular tube or bar under extension, torsion, pressuring, shearing, uniform electric loading and temperature change. Proceedings of the Royal Society of London 458, 2349–2367.

Tarn, J.-Q., Wang, Y.-M., 2001. Laminated composite tubes under extension, torsion, bending, shearing and pressuring: a state space approach. International Journal of Solids and Structures 38, 9053–9075.

Tsukrov, I., Drach, B., 2010. Elastic deformation of composite cylinders with cylindrically orthotropic layers. International Journal of Solids and Structures 47, 25–33.

Wagner, H., 2002. Nanotube-polymer adhesion: a mechanics approach. Chemical Physics Letters 361 (1–2), 57–61.

Wagner, H., Lourie, O., Feldman, Y., Tenne, R., 1998. Stress-induced fragmentation of multiwall carbon nanotubes in a polymer matrix. Applied Physics Letters 72 (2), 188–190.

Wang, Z.L., Gao, R.P., Poncharal, P., de Heer, W.A., Dai, Z.R., Pan, Z.W., 2001. Mechanical and electrostatic properties of carbon nanotubes and nanowires. Materials Science and Engineering C 16, 3–10.

Yakobson, B., Smalley, R., 1997. Fullerene nanotubes: C1,000,000 and beyond. American Scientist 85, review of Nanotubes.

Yakobson, B.I., Campbell, M.P., Brabec, C., Bernholc, J., 1997. High strain rate fracture and c-chain unraveling in carbon nanotubes. Computational Materials Science 8, 341–348.

Yu, M.-F., Files, B.S., Arepalli, S., Ruoff, R., 2000. Tensile loading of ropes of single wall carbon nanotubes and their mechanical properties. Physical Review Letters 84 (24), 5552–5555.

Zhao, Q., Wagner, H.D., 2004. Raman spectroscopy of carbon-nanotube-based composites. Philosophical Transactions of the Royal Society A 362, 2407–2424.

Zhu, J., Kim, J., Peng, H., Margrave, J., Khabashesku, V., Barrera, E., 2003. Improving the dispersion and integration of single-walled carbon nanotubes in epoxy composites through functionalization. Nano Letters 3 (8), 1107–1113.